Mossbauer Spectroscopy

Emily P. Wang
MIT Department of Physics

The ultra-high resolution ($\frac{\Delta E}{E} = 10^{-12}$) method of Mossbauer spectroscopy was used to probe various nuclear effects. The Zeeman splittings of the ground and first excited state of iron-57 were calculated to be spaced apart by $(0.8 \pm 0.2) \times 10^{-7}$eV and $(2.0 \pm 0.3) \times 10^{-7}$eV, respectively. The theoretical values are 1.1×10^{-7} and 1.9×10^{-7}. The ratio between the nuclear magnetic moments of the first excited state and the ground state of the iron-57 atom was calculated to be -1.2 ± 0.3, while the value from literature [1] is -1.715 ± 0.004. The quadrupole splitting of the $3d^6$ state of Fe++ was measured to be $(2.1 \pm 0.5) \times 10^{-7}$eV, while the accepted value is 1.5×10^{-7}eV. The isomer shift in Fe++ was measured to be $(1.7 \pm 0.5) \times 10^{-7}$eV, while the accepted value is 6.7×10^{-8}eV, and the isomer shift in Fe+++ was measured to be$(8 \pm 6) \times 10^{-8}$eV, while the accepted value is 2.4×10^{-8}. The resonant line width was measured to be $6.8 \pm 17.1 \times 10^{-8} eV$, while the accepted value is $4.7 \times 10^{-9} eV$. The lifetime of the first excited state of iron-57 was calculated to be $(6.7 \pm 2.6) \times 10^{-9} seconds$, while the accepted value is 9.8×10^{-8} seconds. The large errors in the resonant line properties can be attributed to the inaccuracy in absolute calibration and error in drive velocity characteristics.

1. INTRODUCTION

The phenomenon of fluorescence was first observed in the mid-1800s by Stokes. Stokes observed that solids, liquids, and gases placed under certain conditions would partially absorb incident electromagnetic radiation that was then re-radiated. A special case of this phenomenon is resonance fluorescence, which occurs when the incident and the re-emitted radiation are of the same wavelength. Scientists were at first prevented from observing resonance absorption on a nuclear level due to the recoil-energy loss of the re-emitted quantum, which caused the emission line to be shifted away from the transition energy required for resonant absorption to occur. Success in observing resonance absorption was eventually obtained through various methods that made use of Doppler shifting to counter the energy shift caused by the recoil. In 1960, Rudolph Mossbauer discovered a method of carrying out "recoilless" spectroscopy by locking the target nuclei into a crystal lattice [2]. Because the crystal lattice's phonons have an extremely low probability absorbing any recoil energy from the incident radiation, all of the excitation energy is transferred to the emitted quantum. These conditions allowed for resonance absorption.

Mossbauer spectroscopy has made possible the probing of the hyperfine structure of an atom, which normally remains obscured by gamma lines, since the thermal width of a gamma line is large in comparison to the spacing of the hyperfine levels of a nucleus. Sharper nuclear transitions, the 14.4keV transition in ^{57}Fe in particular, can be used to measure many important effects [2].

2. THEORY

2.1. Recoil-Free Spectroscopy

The resonant scattering of optical photons has been well-known for many years. The classic example is that of the excitations of sodium vapor, a transition which finds a practical use in fluorescent lighting. In this case, the light quanta emitted by atoms of the emitter, which the transition from their excited states to their ground states are also used to cause the opposite effect in the atoms of an absorber, which consists of identical atoms. The atoms of the absorber undergo a transition from their ground state to their excited states, dropping back down with the emission of fluorescent light [3].

The analogous process in nuclear gamma rays cannot be immediately observed in the same fashion, due to the fact that the gamma ray loses energy to the recoil of the nucleus, causing the emitted gamma ray to have too little energy to be resonantly reabsorbed, since the quantum must provide the kinetic recoil energy in addition to the transition energy [2]. Techniques involving the Doppler shift were used to compensate for this kinetic recoil energy and return the system to resonance conditions.

In 1957, Mossbauer discovered a way of eliminating the problem of recoil by taking advantage of the fact that atoms locked into a crystal lattice cannot recoil arbitrarily. This fact is especially important in regimes where the normal, free-atom recoil energy is comparable to the energy of the quantized lattice vibrations, or phonons. When these conditions exist, it is highly probable for zero-phonon processes to occur. In that case, all of the energy of the incoming gamma ray goes into the nuclear transition, and the recoil momentum is taken by the entire crystal [3]. Mossbauer's method of probing nuclear structure has the unique feature that it insures the complete elimination of energy loss [2].

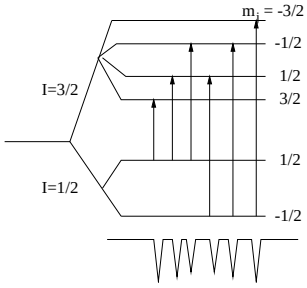

FIG. 1: Diagram of Zeeman splitting and the allowed transitions between the magnetic substates. The arrows indicate that the sample's Fe^{57} electrons in the lower energy substates are excited to higher energy substates when they collide gamma rays of the required energy. The remaining spectrum of gamma rays observed by the detector on the other side of the sample shows absorption peaks at the energies equal to the energies of transition.

2.2. Zeeman Effect in Fe^{57}

When at atom is placed into a magnetic field, its energy lines are split into magnetic substates. This is known as the Zeeman effect. In the Fe^{57} atom, the interaction between the nuclear magnetic moment and the internal magnetic field of the atom allows us to observe Zeeman splitting. The radiation emitted or absorbed in the transition between the ground and 14.4-keV level of Fe^{57} happens to exhibit a clear example of a pure nuclear Zeeman effect. This is due to the fact that there are no additional quadrupole shifts in the nuclear energy levels, due to the cubic symmetry of the iron lattice [1].

The following equation relates g, the Lande constant, to μ, the magnetic moment of the nucleus, and B, the internal magnetic field of the atom: $g_1 = \frac{'mu_1 B}{I_1}$ The equation above gives the relation for the ground state of the Fe^{57} atom, and there is an analogous equation describing the relation for the first excited state of Fe^{57}.

2.3. Resonant Line Width

Due to the Heisenberg uncertainty principle, there is an uncertainty in the energies of the individual excited states of the nuclei, therefore the lines produced by transitions between an excited state and the ground state will have a certain minimum width. This width Γ is called the natural width, and is connected with the lifetime τ of an excited state through the relation $\Gamma = \frac{\hbar \times ln2}{\Gamma}$. Typical values for the lifetimes of lower excited nuclear states range from 10^{-7} to 10^{-11} seconds, which means the natural line widths for ground-state transitions range from 10^{-8} to 10^{-4eV} [2].

2.4. Quadrupole Splitting and Isomer Shift

Quadrupole splitting is a phenomenon that is caused by a nonsymmetric nuclear charge distribution. A nucleus that has a spin quantum number I that is greater than 1/2 will have a non-spherical charge distribution whose magnitude of deformation Q can be expressed as $eQ = \int \rho r^2 (3cos^2\theta - 1) dV$, where e is the charge of a proton, ρ is the charge density in a volume element dV at a distance r from the center of the nucleus and at an angle θ from the nuclear spin quantization axis [4]. Quadrupole splitting serves to lift the degeneracy in the excited states of a nucleus, and the magnitude of the splitting is given by: $\Delta E = eQ \frac{3m_I^2 - I(I+1)}{4I(2I-1)} \frac{\partial^2 \phi}{\partial z^2}$, where ϕ is the electric potential and m_I is the magnetic quantum number of the nuclear state. Quadrupole splitting is not seen in the I= 1/2 ground state of Fe^{57}, but it is seen in the I= 3/2 state, and is given by the expression $\Delta E = \pm \frac{1}{8} Qe \frac{\partial^2 V}{\partial z^2}$

Isomer shift is a nuclear effect that arises from a change in chemical environment between the source and the absorber used in the Mossbauer setup. It involves the interaction between the nuclear charge and the electronic charge within the nuclear volume–specifically, the s electrons, which have a finite charge probability density at the origin, which is where the nucleus of the atom is located. The amount of isomer shift depends on the total electronic charge at the nucleus, which is different in each element [5]. The isomer shift can be calculated with the following equation: $\Delta E = \frac{2\pi}{5} Ze^2 (R_{is}^2 - R_{gs}^2)(|\psi(0)_a|^2 - |\psi(0)_e|^2)$, where Z is the nuclear charge, R_{is} is the radius of the excited electronic state, R_{gs} is the radius of the ground electronic state, $\psi(0)_a$ is the electron wave function of the absorber, $\psi(0)_e$ is the electron wave function of the emitter at $R = 0$.

3. EXPERIMENT

3.1. Michelson Calibration

In order to convert channel (bin) numbers into a meaningful value–namely, the velocity of the drive motor at any given time–it was necessary to do an absolute calibration. This was done with a Michelson interferometer, as shown in Figure 2. The interferometer functioned by recording the interference between different laser beams that reached the photodiode. Interference was caused by the fact that one of the mirrors in the interferometer was attached to the moving drive, thus altering one of the paths taken by the laser. As the drive moves towards and away from the absorber, the photodiode sees a sinusoidal wave that represents the constructive and destructive interference due to the change in path length of the laser beam. When the photodiode signal goes through one cycle of constructive and destructive interference, this means that the drive has traveled a total distance of $\lambda/2$, where λ is the wavelength of the laser. It is $\lambda/2$

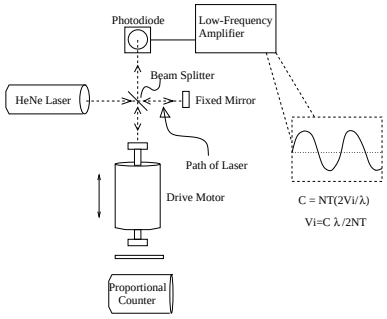

FIG. 2: Setup of the Michelson calibration.

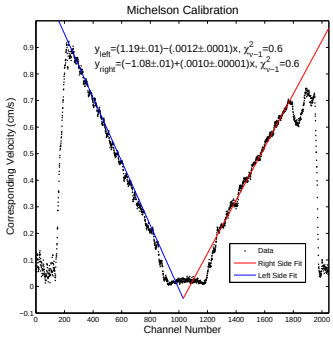

FIG. 3: Calibration data converted to velocity corresponding to each channel, with fit-lines drawn and fit equations shown.

and not *lambda* because the laser beam is reflected at the drive mirror, so a given displacement actually increases the laser path length by twice that displacement. The raw calibration data can be converted from the number of counts in each channel into the drive velocity corresponding to each channel by using the equation $V_i = \frac{C_i \lambda}{2NT}$ where V_i is the velocity corresponding to C_i, the number of counts in the ith channel, N is the number of sweeps made by the drive during a calibration run, and T is the dwell time per channel.

After converting the data from counts to drive velocity, the data was re-plotted fit to two straight lines, as shown in Figure **??**. It is evident from the graph that the drive velocity does not precisely move through the zero velocity point–it has a "blip" that complicates the calibration and the ensuing data analysis, as will be seen shortly.

For our final fit lines, we made the simplifying assumption that the slopes of the fit-lines on either side of the zero velocity point were equal. We averaged the slopes and the x-intercepts of the two lines to obtain the values for the final fit equation. The error in the x-intercept was estimated as half the difference between the two x-intercepts that were averaged (40 channels), added in quadrature to the error due to the blip in the drive velocity (30 channels) for a total error in the x-intercept of 50 channels. The error in the slope was obtained from the original linear fits. The final equation obtained was the following: $V_i = (0.0011 \pm 0.0001)(C_i - 1030 \pm 50)$. This

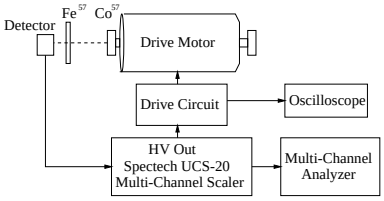

FIG. 4: Schematic of the Mossbauer setup.

equation allowed us to obtain the velocity drive and the energy corresponding the velocity, and therefore a particular channel, could be calculated from the first order Doppler shift equation: $\Delta E = (v/c)E$.

3.2. Zeeman Effect

The setup for this portion of this experiment is shown in Figure **??**. In this portion of the experiment, we observed the effect of Zeeman splitting by observing the difference between the new transition states and the unsplit, single transition state of 14400eV. From this, we can deduce g_0 and g_1, the energy spacings of the split ground state and the split excited state, respectively, and the ratio between μ_0 and μ_1, the magnetic moments of the ground state and the first excited state. Data was obtained by allowing the gamma ray source to impinge upon the Fe^{57} absorber as the drive sweeps through velocities. The raw data was then fit to a six Lorentzian function, and the location of each peak in channel number was noted. The Michelson calibration equation was then used to obtain the drive velocity corresponding to that channel number. The Doppler equation was then used to calculate the ΔE of the transition. The spacings between the split levels, g_0 and g_1, were calculated by taking the differences between the ΔE. The ratio between the magnetic moments of the nucleus was then calculated with the aid of the equation for g_0 and g_1 given in the Theory section above: $\frac{\mu_1}{\mu_0} = \frac{g_1 I_1}{g_0 I_0}$ The Zeeman data was also used as a secondary calibration. Because the Michelson calibration was difficult to carry out, we only performed the absolute calibration once. To scale the velocity fit to data that was taken on the other drive and at other velocities, we compared the Zeeman data taken under different conditions by measuring the differences between the peaks of the six Lorentzians. We then took the ratio of each day's Zeeman data with the original Zeeman data and obtained a different scaling factor for each set of drive conditions. The Zeeman data that was used for obtaining the reference factor is shown in Figure 5.

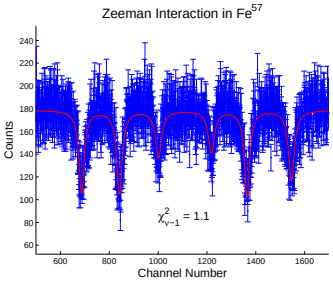

FIG. 5: Zeeman splitting in Fe^{57}

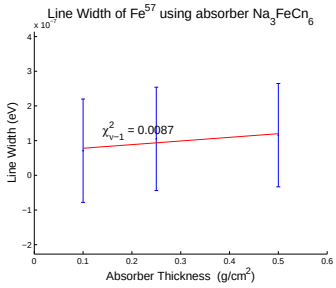

FIG. 6: Resonant line data for absorber at three different thicknesses, plotted with the fitted line.

3.3. Resonant Line Width, Quadrupole Splitting and Isomer Shift

To measure the resonant line width of Fe^{57}, we used the absorber Na_3FeCn_6, which had the advantage that it has no magnetic or electric field gradient at the crystal sites of the iron nuclei. We measured the line width by firing the gamma ray source at the absorber and noting the width of the absorption line that was observed in the multichannel analyzer, using samples of three different thicknesses: 0.1, 0.25, and 0.5g/cm^2. We fit the three line widths to a line and extrapolated to obtain a value of the zero absorber thickness line width of Fe^{57}. From the line width obtained, we calculated the lifetime of the first excited state of Fe^{57}.

To measure both the quadrupole splitting and isomer shift of the $3d^6$ state of Fe++, $Fe(SO_4)$ $7H_2O$ was used as an absorber. The absorber $Fe_2(SO_4)_3$ was used to measure the isomer shift in Fe+++. No quadrupole splitting was observed in Fe+++, as there is no field gradient in the nucleus. The setup was the same as that in the Zeeman splitting portion of this experiment (Figure 4).

4. RESULTS AND ERROR ANALYSIS

4.1. Zeeman and Resonant Line Width

From least to highest energy, the deviations of the six magnetic sub-levels from the unsplit energy were measured to be: $(-1.8 \pm 0.3) \times 10^{-7} eV, (-1.0 \pm 0.3) \times 10^{-7}, (-2.0 \pm 2.6) \times 10^{-8}, (1.0 \pm 0.3) \times 10^{-7}, (1.7 \pm 0.3) \times 10^{-7}, (2.7 \pm 0.3) \times 10^{-7}$. The separations in the split levels were calculated to be $(0.8 \pm 0.2) \times 10^{-7}$eV and $(2.0 \pm 0.3) \times 10^{-7}$eV. The theoretical values for these are 1.1×10^{-7} and 1.9×10^{-7}, as obtained from **??**–the experimental values are both within 2σ of the accepted values, and the second value is within 1σ. The ratio of the magnetic moments of the first excited state to the ground state was calculated to be -1.2 ± 0.3, while the theoretical value is -1.715 ± 0.004; we have good agreement between experimental and accepted values.

We measured the line width at zero absorber thickness to be $6.8 \pm 17.1 \times 10^{-8} eV$, while the accepted value is $4.7 \times 10^{-9} eV$. The lifetime of the first excited state of iron was calculated to be $(6.7 \pm 2.6) \times 10^{-9} seconds$, while the accepted value is 9.8×10^{-8} seconds. The fitted data is shown in Figure 6. The poor reduced chi-squared of the fit is testament, again, to the poor calibration and inaccuracies in the introduced scaling factor.

The uncertainty in the final energy width was calculated by first obtaining the error in the calculated velocity of the drive, since the energy is proportional to the drive velocity by the first order Doppler shift equation. The error in the drive velocity is obtained by the following equation, where s is the scaling factor introduced by comparing Zeeman data taken under different drive conditions, and b is the slope of the final Michelson calibration fit-line:

$$\sigma^2_{V_i} = V_i^2 \left(\frac{\sigma_b^2}{b^2} + \frac{\sigma_s^2}{s^2} + \frac{\sigma^2_{C_i} + \sigma_a^2}{(C_i - a)^2}\right) \quad (1)$$

We found that most of the error was obtained from the error in the x-intercept, σ_a, which is hardly surprising, as there was significant uncertainty in the absolute calibration around the zero velocity channel.

4.2. Quadrupole Splitting and Isomer Shift

The quadrupole splitting of the $3d^6$ state of Fe++ was measured to be $(2.1 \pm 0.5) \times 10^{-7}$eV, while the accepted value is 1.5×10^{-7}eV. The isomer shift in Fe++ was measured to be $(1.7 \pm 0.5) \times 10^{-7}$eV, while the accepted value is 6.7×10^{-8}eV, and the isomer shift in Fe+++ was measured to be$(8 \pm 6) \times 10^{-8}$eV, while the accepted value is 2.4×10^{-8}. In doing the data analysis for this portion of the experiment, it was necessary to eliminate part of the raw data, as there was unwanted noise generated y the drive velocity error, as shown in Figure 7, where the characteristic of the raw data deviates from a Lorentzian. The error was determined to span an area of (100 ± 30) channels and was cut out of the data. Upon reshifting the data and refitting, it was found that the Lorentzian fits now achieved favorable reduced chi-squared values that were close to unity. The isomer shift data sets were used to estimate the area spanned by the area, as the noise was easiest to make out in those data sets. The

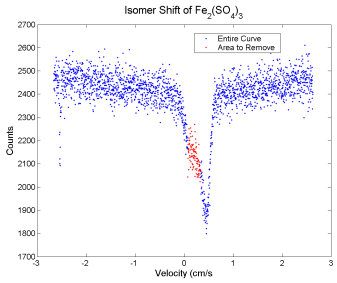

FIG. 7: Raw data for isomer shift in Fe+++ before correction.

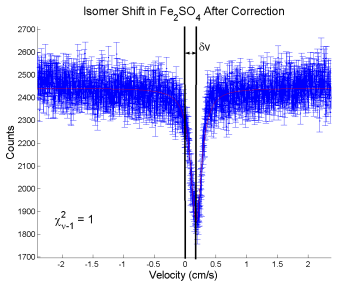

FIG. 8: Data for isomer shift after correction.

same area of channels were cut out of both isomer and quadrupole splitting data (Figures 8 and 9.

5. CONCLUSIONS

Using the recoilless method of Mossbauer spectroscopy, we were able to observe the Zeeman splittings in Fe^{57} and calculate the separations in the energy splittings of the ground and first excited state, $(0.8 \pm 0.2) \times 10^{-7}$eV and $(2.0 \pm 0.3) \times 10^{-7}$eV respectively, which compare well with the theoretical values, 1.1×10^{-7} and 1.9×10^{-7} respectively. The ratio of the nuclear magnetic moments of the first excited state and the ground state, $\frac{\mu_1}{\mu_0}$, was calculated to be -1.2 ± 0.3, while the value from literature [1] is -1.715 ± 0.004–again, there is good agreement between experiment and theory. The quadrupole splitting of the $3d^6$ state of Fe++ was measured to be

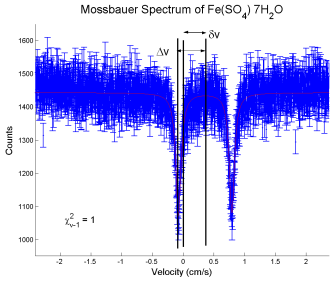

FIG. 9: Data for combined quadrupole effects in Fe++ after correction.

$(2.1 \pm 0.5) \times 10^{-7}$eV which is within 2σ of the accepted value, 1.5×10^{-7}eV. The isomer shift in Fe++ was measured to be $(1.7 \pm 0.5) \times 10^{-7}$eV, while the accepted value is 6.7×10^{-8}eV. The isomer shift in Fe+++ was measured to be$(8 \pm 6) \times 10^{-8}$eV, while the accepted value is 2.4×10^{-8}. The resonant line width data showed poor agreement between experiment and theory. The resonant line width was measured to be $6.8 \pm 17.1 \times 10^{-8} eV$, while the accepted value is $4.7 \times 10^{-9} eV$. The lifetime of the first excited state of iron-57 was calculated to be $(6.7 \pm 2.6) \times 10^{-9} seconds$, while the accepted value is 9.8×10^{-8} seconds. The discrepancy is large–over an order of magnitude–and is due to the inaccurate Michelson calibration and, to a lesser degree, inaccuracies in the secondary Zeeman calibration. One unaccounted error was the error in the scaling factor c, which varied by 10% between days. There is also error involved in the convolution between the source and absorber–this is due to the fact that the source and absorber are not point objects, but have a finite area. This would lead to line broadening in the data collected. In order to improve accuracy in this experiment, it is imperative that the absolute calibration be improved. This could be done by taking the Michelson calibration under every different drive condition used to collect data. Also, another possibility is making improvements to the drive velocity characteristic and eliminating the "blip".

[1] H. et. al, *Mossbauer effect in metallic iron* (1962).
[2] R. L. Moessbauer, *Nobel lecture: Recoilless nuclear resonance absorption of gamma radiation* (1961).
[3] J. King, *Mossbauer effect: Selected reprints* (1963).
[4] D. J. Bland, *Electric quadrupole splitting*, URL `http://www.cmp.liv.ac.uk/frink/thesis/thesis/node18.html`.
[5] Boyle and Hall, *The mossbauer effect (reports on the progress of physics).*

Acknowledgments

The author would like to acknowledge Kelley Rivoire, her fellow investigator, and the junior lab staff for their assistance in lab.